RF MEMS Integrated Frequency Reconfigurable Annular Slot Antenna

Bedri A. Cetiner, *Member, IEEE*, Gemma Roqueta Crusats, *Student Member, IEEE*, Lluís Jofre, *Senior Member, IEEE*, and Necmi Bıyıklı, *Member, IEEE*

***Abstract*—A new kind of double- and single-arm cantilever type DC-contact RF MEMS actuators has been monolithically integrated with an antenna architecture to develop a frequency reconfigurable antenna. The design, microfabrication, and characterization of this "reconfigurable antenna (RA) annular slot" which was built on a microwave laminate TMM10i (ε_r = 9.8, $\tan\delta$ = 0.002), are presented in this paper. By activating/deactivating the RF MEMS actuators, which are strategically located within the antenna geometry and microstrip feed line, the operating frequency band is changed. The RA annular slot has two reconfigurable frequencies of operation with center frequencies f_{low} =2.4 GHz and f_{high} = 5.2 GHz, compatible with IEEE 802.11 WLAN standards. The radiation and impedance characteristics of the antenna along with the RF performance of individual actuators are presented and discussed.**

***Index Terms*—Full-wave analyses, microfabrication, reconfigurable antenna, RF MEMS actuators.**

I. Introduction

THE reconfigurable antenna (RA) concept [1], [2] has gained significant interest as a result of two main factors. First, a single RA can perform multiple functions by dynamically changing its properties (operating frequency, polarization, and radiation pattern). This can result in a significant reduction in the overall size of multi-mode multi-band wireless communication systems and replace multiple single-function legacy antennas. Second, the reconfigurable antenna properties of a RA can be used as important additional degrees of freedom in an adaptive system (first proposed in [3] and later in [4]–[7]). In particular it was shown that a RA equipped adaptive multiple-input multiple-output (MIMO) wireless communication system can provide gains up to 30 dB as compared to conventional fixed antenna MIMO systems [7]. These additional gains result from the joint optimization of dynamically reconfigurable antenna properties with adaptive space-time modulation techniques [8] in response to the changes in the propagation environment.

Manuscript received January 29, 2009; revised April 28, 2009. First published December 28, 2009; current version published March 03, 2010. This work was supported in part by Army Research Office under Grant W911 NF-07-1-0208 and in part by the National Institute of Justice, Office of Justice Programs, US Department of Justice under Grant 2007-IJ-CX-K025.

B. A. Cetiner and N. Bıyıklı are with the Electrical and Computer Engineering Department, Utah State University, Logan, UT 84322 USA (e-mail: bedri@engineering.usu.edu).

L. Jofre and G. Roqueta Crusats are with the Department of Signal Theory and Communications, Technical University of Catalonia, 08034 Barcelona, Spain.

Color versions of one or more of the figures in this paper are available online at http://ieeexplore.ieee.org.

Digital Object Identifier 10.1109/TAP.2009.2039300

In order to dynamically change the properties of a RA, the current distribution over the volume of the antenna needs to be changed, where each distribution corresponds to a different mode of operation. To this end, one can change the geometry and feed line of the antenna by switching on and off various geometrical segments that make up the RA and the feed circuitry. For switching, either MEMS or solid-state switching devices can be employed. In this work, we prefer using RF MEMS actuators due to monolithic integration capability with antenna segments along with their low loss and power characteristics. Also, the potential of MEMS in avoiding nonlinearity and intermodulation effects is an important advantage over solid-state switching devices [9].

To cover multiple frequency bands by a single antenna element, various design approaches such as a multi-frequency antenna covering each individual band, a broadband antenna covering the whole frequency bandwidth, or a RA with a narrow instantaneous operating bandwidth that can be tuned over the whole bandwidth can be used. The design of slot-ring antennas for mobile communications was previously studied in [10], [11]. Multi-frequency operation was also presented in several research papers. In [12], [13], the multi-band operation is achieved by using multiple concentric annular-ring slots, which are fed by either a microstrip or coplanar waveguide. Microstrip-fed slot-ring antennas, which consist of a single slot-ring of various geometries, that achieve multi-frequency operation were also investigated [14]. Although these antennas support multiple frequencies, the radiation patterns and gain values corresponding to each frequency can be significantly different. The same problem applies to a broadband antenna, where the degradation in gain can be significant over a broad frequency band. This might be a problem for multi-mode multi-band wireless communications applications where the radiation characteristics and gain performance are required to be similar over multiple frequencies. Recent efforts have been focusing on the tunable slot-ring antennas [15], [16]. The RA annular slot presented in this paper maintains the same radiation characteristics for both modes of operation ($f_{\text{low}} = 2.4$ GHz and $f_{\text{high}} = 5.2$ GHz) due to a similar tunable highly efficient operating bandwidth over which the radiation behavior remains almost constant. This is accomplished by MEMS reconfiguration which provides a circular one-wavelength-perimeter for both the external longer slot of the lower frequency and the internal shorter one of the higher frequency band. Additionally the use of an annular geometry compared to the conventional linear slot reduces the dimension of the antenna by a $2/\pi$ factor (perimeter of λ for the annular slot instead of a length of $\lambda/2$ for the linear slot).

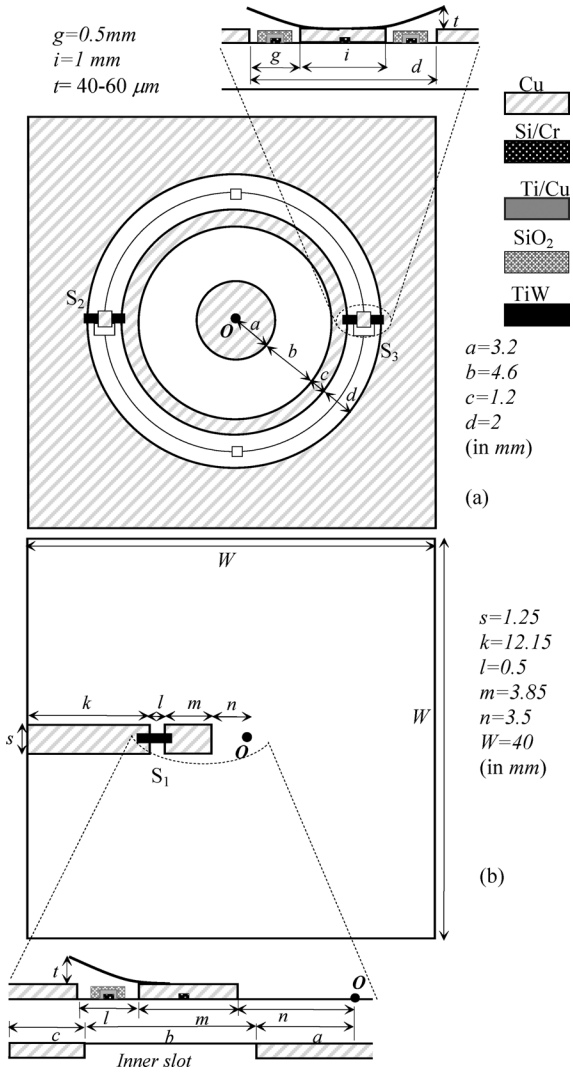

Fig. 1. Architecture of the microstrip-fed RA annular slot. (a) Top view and magnified A-A' cross section view. (b) Bottom view and magnified B-B' cross section view. (MEMS actuator width is 350 μm and length is 650 μm).

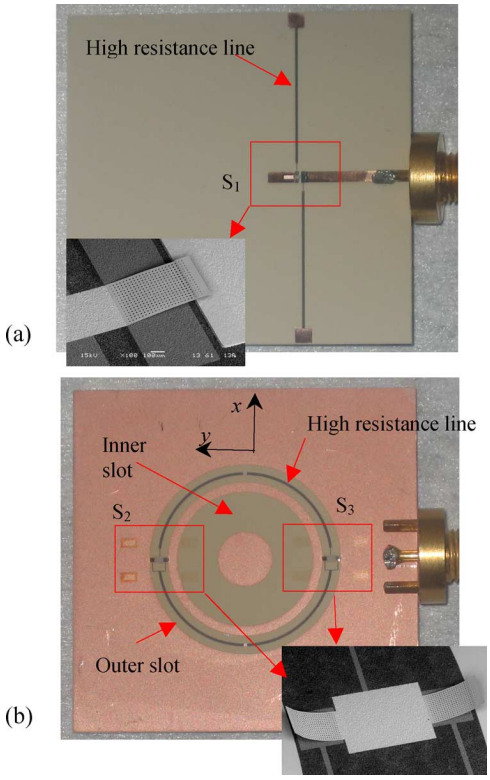

Fig. 2. Photograph of the RA annular slot. (a) Microstrip feed line integrated with a single-arm MEMS actuator. (b) Annular slot integrated with two double-arm MEMS actuators.

II. Reconfigurable Annular Slot: Architecture, Design, Characterization

A. Architecture and Working Mechanism

The architecture and a photograph of the microstrip-fed RA annular slot are shown in Figs. 1 and 2, respectively.

The antenna is built on two separate layers of TMM10i ($\varepsilon_r = 9.8$, $\tan\delta = 0.002$) microwave laminate each with 0.635 mm thickness. The microstrip feed line is placed on one layer and the annular slot is placed on the other layer, which are bonded together having a total thickness of 1.27 mm. This RA has two concentric circular slots, each of which can be excited individually in order to achieve frequency reconfigurability. The microstrip feed line is broken into two segments, which are spanned by a single-arm cantilever type MEMS actuator, S_1 (see Fig. 1(b) and the inset of Fig. 2(a) for a magnified view), which is similar to the MEMS switch presented in [17]. The actuator S_1 enables either the outer or the inner slot to be excited by changing the length of the microstrip. When S_1 is not activated (actuator up-state), the microstrip segments are disconnected, thereby the outer slot is fed; the operation frequency is $f_{\text{low}} = 2.4$ GHz (Mode 1). When S_1 is activated (actuator down-state), the microstrip segments become connected, thereby the inner slot is fed; the operation frequency is $f_{\text{high}} = 5.2$ GHz (Mode 2). Two double-arm cantilever type MEMS actuators, S_2 and S_3 (see Fig. 1(a) and inset of Fig. 2(b) for a magnified view), are located on the opposite sides of the outer slot as shown in Figs. 1(a) and 2(b). These actuators enable the metallic annular ring, which stays between the outer and inner slots, to be shorted to RF ground so that when the inner slot is excited, it has a continuous ground plane. Therefore the operation of the inner slot is not adversely impacted by the presence of the outer slot. We also observed that when the outer slot is excited for $f_{\text{low}} = 2.4$ GHz, the influence of the presence of the inner slot combined with the central metallic circular island on the outer slot produces only a minor resonant effect, which is out of the operation range of the higher frequency, thereby not requiring the inner slot to be shorted.

The actuation of the MEMS actuators is due to the electrostatic force created by the applied DC voltage between the cantilever's metallic post (the fixed point of the MEMS actuator) and the pull-down bias electrode which is placed underneath the cantilever. When the applied electrostatic force becomes larger than the mechanical force due to the stress of the metallic cantilever beam, the cantilever moves down and makes a DC contact, thereby connecting the broken microstrip segments and also creating a short to the ground plane. DC bias voltages are applied through high DC resistance Silicon Chrome (SiCr) lines with a sheet resistance of approximately 50 kΩ/square and an

absolute resistance of 500 $\mathrm{k}\Omega$. Please note that the bias line used to activate S_2 and S_3 is placed into the outer slot for the compactness of the design. Due to high resistivity of the bias line, this placement has no detrimental effect to the operation of RA annular slot as demonstrated by the measurements and simulations given in the following sections.

An annular slot etched in a large conducting plane can be viewed as an annular distribution of a magnetic current given by the actual mode excited into the circumferential slot. To obtain maximum bandwidth with minimum dimensions, the TM_{11} mode, normally called fundamental mode, tends to be the basic choice [18]. Considering the annular slot as a transmission line, the fundamental resonance appears around the frequency at which the circumference of the annular slot becomes one guided wavelength of the slot (λ_{gs}). The slot guided wavelength for the frequency and dielectric permittivity ranges of interest can be expressed [19] as

$$\frac{\lambda_{gs}}{\lambda_o} = 0.9217 - 0.277\ln\varepsilon_r + 0.0322\left(\frac{w}{h}\right)\left[\frac{\varepsilon_r}{\frac{w}{h}+0.435}\right]^{1/2} - 0.01\ln\left(\frac{\mathrm{h}}{\lambda_o}\right)\left[4.6 - \frac{3.65}{\varepsilon_r^2\sqrt{\frac{w}{\lambda_o}}\left(9.06 - 100\left(\frac{w}{\lambda_o}\right)\right)}\right] \quad (1)$$

where w is the slot-line width, λ_0 the free-space wavelength, and ε_r and h are the permittivity and thickness of the substrate, respectively. While (1) provides a good first order approximation for the resonance frequency, the actual frequency for the microstrip-fed MRA annular slot will be in close vicinity of that of given by (1) as the penetration distance of the projection of the microstrip onto the slot plays a second order role on the resonance frequency. As seen in Fig. 1(b), this penetration distance for the inner slot is $(a+b)-n$. The bandwidth may be adjusted by selecting the appropriate internal and external radii of the slots as

$$\frac{f_i^{(2)} - f_i^{(1)}}{f_i^{(0)}} = \frac{R_i^{(2)} - R_i^{(1)}}{R_i^{(0)}} \quad (2)$$

where $f_i^{(0)}$, $f_i^{(1)}$, $f_i^{(2)}$ are the central, upper and lower frequencies for the $i = \text{low}$ or $i = \text{high}$ frequency bands and $R_i^{(0)}$, $R_i^{(1)}$, $R_i^{(2)}$ are the central, external and internal radius for the $i = \text{low}$ (outer slot) or $i = \text{high}$ (inner slot) frequency bands. Please note that these definitions indicate that $R_i^{(0)} \approx \lambda_{i,gs}$, where $\lambda_{i,gs}$ is the guided wavelength corresponding to $i = \text{low}$ (outer slot) or $i = \text{high}$ (inner slot) frequency bands.

B. Microfabrication

The microfabrication process of the RA annular slot was performed based on the microwave laminate compatible RF MEMS technology [1], [20], [22] that enables the monolithic integration of MEMS actuators with antenna segments. The layout of MEMS actuators and antenna segments including microstrip feed lines and high resistance DC control lines are part of the same lithographic process. Thus, the process flow for a single double-arm MEMS actuator interconnecting two different antenna metallic segments is given in Fig. 3, which also serves as the description for the complete microfabrication of the RA annular slot. Because this RA has MEMS actuators on both sides of the substrate, the two sides are processed separately and subsequently bonded together. We developed a seven-step microfabrication process using microwave laminate TMM10i substrates. The microfabrication process was started by wet-etching and chemical mechanical polishing (CMP) the 15 μm-thick Cu layer on top of the microwave laminate TMM10i substrate down to ~ 2 μm. Afterwards, the annular slot and microstrip line segments were patterned and wet-etched selectively. Next, ~ 200 nm-thick SiCr bias lines were formed by DC-sputtering which was followed by the formation of Ti/Cu bias electrode pads. A ~ 2 μm thick Ti/Cu island metal is deposited as the central-base metallic pad for the MEMS cantilever beam. In the fifth step, bias lines and bias electrodes were passivated with a 250 nm thick SiO_2 dielectric layer. This was followed by the deposition of a thick (~ 3 μm) amorphous Si (a:Si) sacrificial layer which was planarized using CMP. In the final seventh step, a ~ 1.0 μm thick TiW layer was sputtered. After dry-release process, the cantilevers (width $= 350$ μm and length $= 650$ μm) curled upwards due to the internal stress-gradient within the deposited TiW. Fig. 3 summarizes the microfabrication process steps used for double-arm MEMS actuators interconnecting two metal segments of RA annular slot structure.

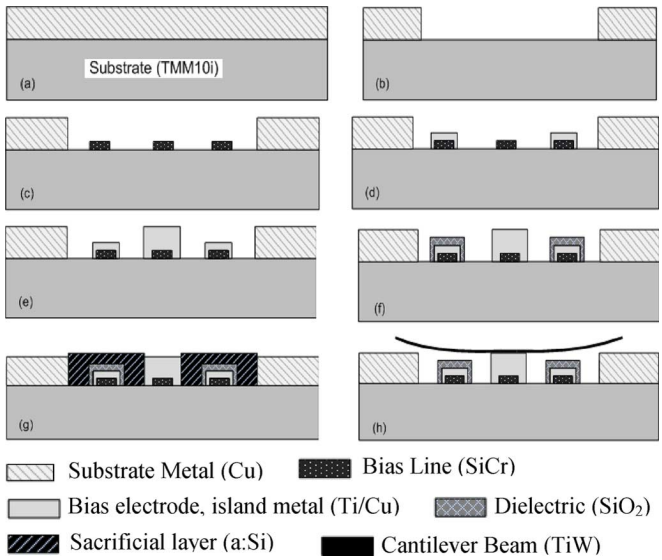

Fig. 3. Microfabrication process steps for the double-arm MEMS actuator interconnecting two segments of the RA annular slot.

It is important to note that a MEMS integrated antenna needs to be packaged since it is exposed to harsh environmental conditions when in use. To seal the entire MEMS integrated antenna structure, a wafer scale low-loss packaging technology, which was recently developed by MIT Lincoln Laboratory [23], can be used.

1) RF Characterization of RF MEMS Single- and Double-Arm Actuators: RF performances of the individual single- and double-arm actuators have been characterized by measuring and simulating small-signal S-parameters. To this

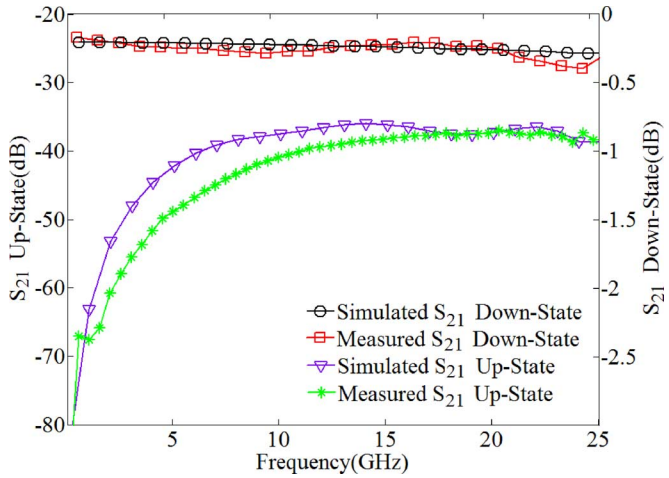

Fig. 4. Measured and simulated S_{21} of the double-arm MEMS actuator.

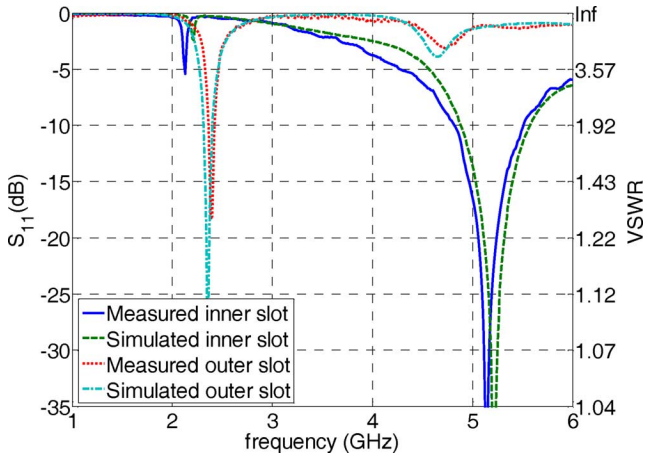

Fig. 5. Measured and simulated reflection coefficients for $f_{\text{high}} = 5.2$ GHz (Mode 2 operation, inner slot is excited), and for $f_{\text{low}} = 2.4$ GHz (Mode 1 operation, outer slot is excited).

end, an RF-probe station interfaced to a vector network analyzer is used. The results for single- and double-arm actuators are observed to be very similar, therefore only double-arm actuator results are given in Fig. 4. As shown in Fig. 4, the average value of S_{21}, in the down-state, including the inherent loss of the microstrip ($S_{21} < -0.1$ dB) is ~ -0.25 dB over the frequency range of 500 MHz to 25 GHz. The corresponding switch contact resistance is $\sim 2\,\Omega$, which can be found by using $S_{21} = 2Z_o/(2Z_o + R_c)$, where R_c is the switch resistance and Z_o ($= 50\,\Omega$) is the characteristic impedance of the microstrip. S_{21} in the up-state ranges from -80 dB to -40 dB for the same frequency range. The actuation voltage was at around 20 Volts.

C. Reflection Coefficient

To measure the antenna reflection coefficients, i.e., the S_{11} parameter, corresponding to Mode 1 and Mode 2 operations, the RA annular slot was connected to the fully-calibrated single port of a VNA. For Mode 2 operation ($f_{\text{high}} = 5.2$ GHz) MEMS actuators were activated (actuators down-state) by applying DC bias voltages. In the case of Mode 1 operation ($f_{\text{low}} = 2.4$ GHz), the actuators were in the up-state not requiring DC bias. The measured and simulated reflection coefficients, with a good agreement between them, corresponding to two reconfigurable modes of operation, $f_{\text{high}} = 5.2$ GHz and $f_{\text{low}} = 2.4$ GHz, are shown in Fig. 5. For a 1:2 VSWR (~ -10 dB reflection coefficient), the corresponding frequency bandwidths are 100 MHz and 650 MHz for 2.4 GHz and 5.2 GHz, respectively, covering the ISM allocated frequency range. For each mode of operation a small amount of residual resonance of the non-activated slot appears, which is due to the different feeding-boundary conditions created by the presence of the activated MEMS. The small residual resonance, however, is out of the active band with negligible effect on the antenna performance.

D. Radiation Patterns and Current Distribution

Antenna radiation pattern measurements have also been performed for Modes 1 and 2. The measurements took place in an anechoic chamber at $f_{\text{low}} = 2.4$ GHz (Mode 1) and $f_{\text{high}} = 5.2$ GHz (Mode 2) frequencies in the principal cuts, E- and H-planes, which correspond to y-z ($\phi = 90$) and x-z ($\phi = 0$) planes, respectively. Both co- and cross-polar components were measured and compared to the simulated results, which were obtained using [24]. At each frequency, the radiation pattern in the E and H planes are normalized with respect to the maximum in their crossing points. The results for $f_{\text{low}} = 2.4$ GHz and $f_{\text{high}} = 5.2$ GHz are shown in Figs. 6 and 7, respectively. The measured and simulated results agree well. Well-behaved linear polarization and broadside radiation patterns are observed, and the two frequencies have the same polarization planes. Cross-polarization levels at both planes remain quite low, on the order of -20 dB, due to the geometrical symmetry especially with respect to the y-axis.

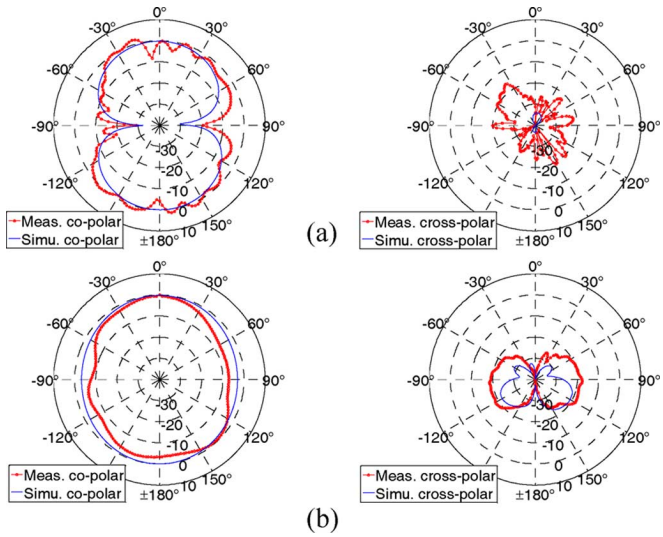

Fig. 6. Co- and cross-polar radiation patterns at $f_{\text{low}} = 2.4$ GHz (a) in E-plane(y-z plane, $\phi = 90$), (b) in H-plane (x-z plane, $\phi = 0$).

The electric field distributions on the inner and outer slots have also been studied. Fig. 8(a) and (b) show the simulated current distribution at $f_{\text{low}} = 2.4$ GHz and $f_{\text{high}} = 5.2$ GHz, respectively. The electric field distributions are similar to each other resulting in similar radiation patterns at both frequencies as shown in Figs. 6 and 7.

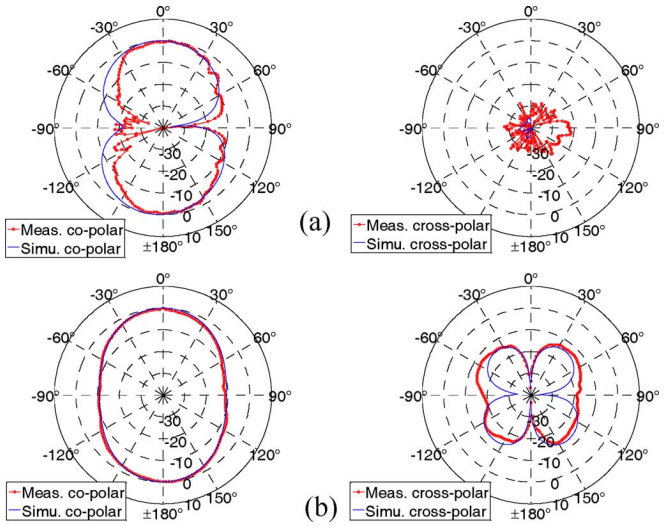

Fig. 7. Co- and cross-polar radiation patterns at $f_{\text{high}} = 5.2$ GHz (a) in E-plane(y-z plane, $\phi = 90$), (b) in H-plane (x-z plane, $\phi = 0$).

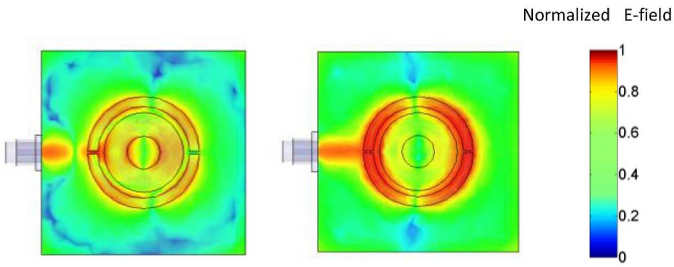

Fig. 8. Electric field distributions on the RA annular slot for (a) Mode 2, $f_{\text{high}} = 5.2$ GHz and (b) Mode 1, $f_{\text{low}} = 2.4$ GHz.

The gain values corresponding to both modes of operation have been determined from the product of ohmic efficiency (η_l), directivity (D) and the mismatch factor $(1 - |S_{11}|^2)$, $G = \eta_l D(1 - |S_{11}|^2)$. The directivities have been obtained by integration of the three-dimensional measured radiation patterns with 3° angular step with an accuracy of ± 0.5 dB (resulting from the combination of the measurement and integration relative errors: $\delta_{\text{measurement}} = \pm 0.05$, $\delta_{\text{integration}} = \pm 0.01$ obtained from a set of measurements for different distances and angular steps). In order to measure the efficiency of the antenna avoiding the influence of the feeding cables that the limited ground plane (in the order of 0.3 wavelengths at the lower frequency) could produce, the antenna has been vertically mounted into a large ground plane, enclosed by a cap. The Wheeler cap method has then been used to determine the ohmic efficiency with a precision of ± 0.2 dB

$$\eta_l = \frac{\text{Re}\{Z_{in}\} - \text{Re}\{Z_{wc}\}}{\text{Re}\{Z_{in}\}} \tag{3}$$

where Z_{wc} is the input impedance of the antenna while it is placed inside the Wheeler cap, and Z_{in} is the input impedance without the cap. The results are summarized in Table I.

As expected gain values close to 2.7 dB for the inner and 2 dB for the outer slots are obtained with combined precision of ± 0.6 dB resulting from the combination of directivity and efficiency estimated accuracies. In order to check these results, especially at the lower frequency band where the effects of the cables and finite ground plane may be more significant, a direct band-limited measurement of the gain has been performed with a far-field anechoic chamber. In summary, the RA annular slot has similar gain and well behaved radiation patterns at both frequency bands, which is a required antenna property for multi-mode multi-band mobile wireless communication applications.

TABLE I
DIRECTIVITY, EFFICIENCY AND GAIN VALUES OF THE RA ANNULAR SLOT WITH AND WITHOUT BIAS LINE

		Directivity D	Efficiency η	Gain G
Wheeler Cap	Inner slot w/o bias line (5.2 GHz)	3.10 dB	0.93	2.78 dB
	Inner slot with bias line (5.2 GHz)	3.12 dB	0.92	2.75 dB
	Outer slot w/o bias line (2.4 GHz)	2.30 dB	0.96	2.12 dB
	Outer slot with bias line(2.4 GHz)	2.31 dB	0.90	1.85 dB
Far Field Meas.	Outer slot w/o bias line (2.35 - 2.45 GHz)			2.1±0.1dB
	Outer slot with bias line (2.35 - 2.45 GHz)			1.8 ±0.1dB

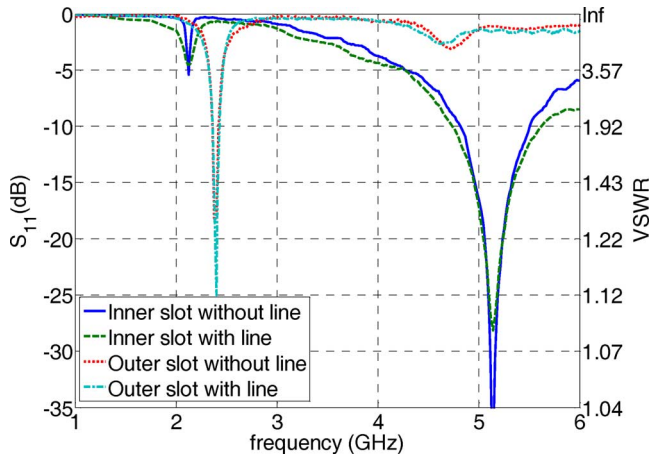

Fig. 9. Measured reflection coefficients with and without the bias lines at Mode 1 and Mode 2 of operation.

E. The Influence of the Bias Circuitry on the MRA Performance

A RA with MEMS actuators monolithically integrated within radiating antenna segments requires an effective DC biasing approach to achieve both actuator actuation and decoupling between radiating antenna and DC control signals. In this work, a high DC resistance line approach is implemented as opposed to high RF impedance conductive metal lines, since the latter can cause deleterious electromagnetic interactions degrading the antenna performances. As described in the microfabrication section, high DC resistance lines of Silicon Chrome (SiCr) with a sheet resistance of approximately 50 $\text{k}\Omega/\text{square}$ and an absolute resistance of 500 $\text{k}\Omega$ are used.

In order to investigate the influence of DC bias lines on the antenna performances, radiation patterns and reflection coefficients were measured for both modes of operation (Mode 2: $f_{\text{low}} = 5.2$ GHz and Mode 1: $f_{\text{high}} = 2.4$ GHz) for the two cases: with and without bias lines. The comparative results shown in Figs. 9–11 indicate that the influence of the bias line

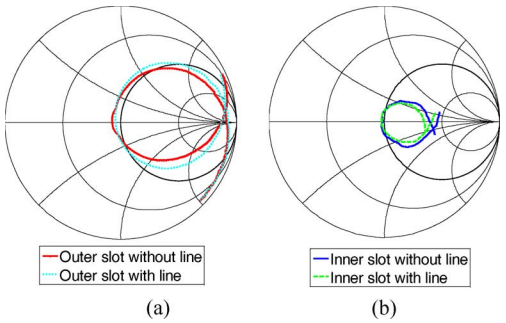

Fig. 10. Band-limited Smith chart representation with and without the bias lines at (a) Mode 1 (2 – 3 GHz) and (b) Mode 2 (4.5 – 5.5 GHz).

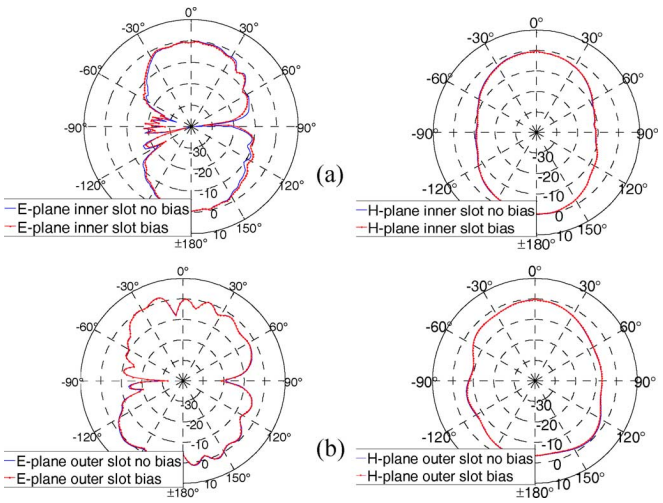

Fig. 11. Measured co-polar radiation patterns in E- plane (y-z plane, $\phi = 90$) and in H-plane (x-z plane, $\phi = 0$) with and without bias lines at (a) 5.2 GHz (Mode 2) and (b) 2.4 GHz (Mode 1).

on both the impedance (magnitude and phase) and the radiation behavior is negligible.

III. Conclusion

A frequency reconfigurable ($f_{\text{low}} = 2.4$ GHz and $f_{\text{high}} = 5.2$ GHz) annular slot antenna has been designed, microfabricated, and characterized. The reconfigurability is achieved through single- and double-arm DC-contact MEMS actuators, which are strategically located within the antenna geometry and the microstrip feed line. Simulations and measurements showed that the antenna has similar gain (~ 2 dB) and well behaved radiation patterns at both frequency bands, which is a required antenna property for multi-mode multi-band mobile wireless communication applications. The average value of S_{21} (~ -0.2 dB in the switch down-state) indicates that the switch contact resistance is $\sim 2\ \Omega$. Furthermore, the effect of SiCr bias circuitry on the radiation and impedance characteristics has been found to be negligible.

Acknowledgment

This work was performed in part at the Cornell NanoScale Facility (CNF), a member of the National Nanotechnology Infrastructure Network, which is supported by the National Science Foundation.

References

[1] B. A. Cetiner *et al.*, "Monolithic integration of RF MEMS switches with a diversity antenna on PCB substrate," *IEEE Trans. Microw. Theory Tech.*, vol. 51, no. 1, pp. 332–335, Jan. 2003.

[2] Y. Rahmat-Samii and C. Christodoulou, Eds., *IEEE Trans. Antennas Propag., Special Issue on Multifunction Antennas and Antenna Systems*, vol. 54, pt. 1, Feb. 2006.

[3] B. A. Cetiner *et al.*, "Multifunctional reconfigurable MEMS integrated antennas for adaptive MIMO systems," *IEEE Commun. Mag.*, vol. 42, pp. 62–70, Dec. 2004.

[4] B. Akbar, M. Sayeed, and V. Raghavan, "Maximizing MIMO capacity in sparse multipath with reconfigurable antenna arrays," *IEEE J. Sel. Topics Signal Processing*, vol. 1, no. 1, pp. 156–166, Jun. 2007.

[5] D. Piazza *et al.*, "Design and evaluation of a reconfigurable antenna array for MIMO systems," *IEEE Trans. Antennas Propag.*, vol. 56, pp. 869–881, 2008.

[6] A. Grau, H. Jafarkhani, and F. De Flaviis, "Reconfigurable MIMO communication system," *IEEE Trans. Wireless Commun.*, vol. 7, no. 5, pp. 1719–1733, May 2008.

[7] B. A. Cetiner, E. Sengul, E. Akay, and E. Ayanoglu, "A MIMO system with multifunctional reconfigurable antennas," *IEEE Antennas Wireless Propag. Lett.*, vol. 5, pp. 463–466, Dec. 2006.

[8] S. Catreux *et al.*, "Adaptive modulation and MIMO coding for broadband wireless data networks," *IEEE Commun. Mag.*, vol. 40, no. 6, pp. 108–15, Jun. 2002.

[9] G. M. Rebeiz, *RF MEMS: Theory, Design and Technology*. New York: Wiley, 2003.

[10] P. Mastin, B. Rawat, and M. Williamson, "Design of a microstrip annular slot antenna for mobile communications," in *Proc. IEEE Antennas Propag. Symp.*, Jul. 1992, vol. 1, pp. 507–510.

[11] L. Lavi and J. Liva, "Wide-bandwidth circularly polarized array consisting of linearly polarized annular slots and parasitic microstrip patches," in *Proc. IEEE Antennas Propag. Symp.*, Jun. 1991, vol. 2, pp. 638–641.

[12] J.-S. Chen, "Multi-frequency characteristics of annular-ring slot antennas," *Microw. Opt. Technol. Lett.*, vol. 38, no. 6, pp. 506–511, Sep. 2003.

[13] X. Qing and M. Chin, "Broadband annular dual-slot antenna for WLAN applications," in *Proc. IEEE Antennas and Propag. Int. Symp.*, 2002, vol. 2, pp. 452–455.

[14] H. Tehrani and K. Chang, "Multifrequency operation of microstrip-fed slot-ring antennas on thin low-dielectric permittivity substrates," *IEEE Trans. Antennas Propag.*, vol. 50, pp. 1299–1308, Sep. 2002.

[15] I. Carrasquillo-Rivera *et al.*, "Tunable and dual-band rectangular slotring antenna," in *Proc. IEEE Antennas Propag. Symp.*, Jun. 2004, vol. 4, pp. 4308–4311.

[16] C. R. White and G. M. Rebeiz, "Single- and dual-polarized tunable slot-ring antenna," *IEEE Trans. Antennas Propag.*, vol. 57, no. 1, pp. 439–448, Jan. 2009.

[17] S. Duffy, C. O. Bozler, S. Rabe, J. Knecht, L. Travis, P. W. Wyatt, C. L. Keast, and M. Gouker, "MEMS microswitches for reconfigurable microwave circuitry," *IEEE Microw. Wireless Compon. Lett.*, vol. 11, pp. 106–108, Mar. 2001.

[18] R. Garg, P. Barthia, I. Bathl, and A. Ittipibon, *Microstrip Antenna Design Handbook*. Boston, MA: Artech House, 2001.

[19] R. Janaswamy and D. H. Schaubert, "Characteristic impedance of a wide slotline on low permittivity substrates," *IEEE Trans. Microw. Theory Tech.*, vol. MTT-34, pp. 900–902, Aug. 1986.

[20] B. A. Cetiner, H. P. Chang, J. Y. Qian, M. Bachman, F. De Flaviis, and G. P. Li, "MEMS fabrication on a laminated substrate," U.S. patent 7,084,724 B2, Aug. 1, 2006.

[21] H. P. Chang *et al.*, "Design and process consideration for fabricating RF MEMS switches on printed circuit boards," *IEEE J. MEMS*, vol. 14, no. 6, pp. 1311–1322, Dec. 2005.

[22] B. A. Cetiner and N. Biyikli, "Penta-band planar inverted F-antenna (PIFA) integrated by RF NEMS switches," presented at the IEEE University Government Industry Micro/Nano Symp., Louisville, KY, Jul. 13–18, 2008.

[23] J. Muldavin, C. O. Bozler, S. Rabe, P. W. Wyatt, and C. L. Keast, "Wafer-scale packaged RF microelectromechanical switches," *IEEE Trans. Microw. Theory Tech.*, vol. 56, no. 2, pp. 522–529, Feb. 2008.

[24] "Ansoft HFSS Version 11, 3D EM-Field Simulation for High Performance Electronic Design,". Pittsburgh, PA, Ansoft Corporation.

Bedri A. Cetiner (M'00) received the Ph.D. degree in electronics and communications engineering from the Yildiz Technical University, Istanbul, in 1999.

From November 1999 to June 2000, he was with the University of California, Los Angeles, as a NATO Science Fellow. He then joined the Department of Electrical Engineering and Computer Science, University of California, Irvine, where he worked as a Research Specialist from June 2000 to June 2004. From July 2004 until July of 2007, he worked as an Assistant Professor in the Department of Space Science and Engineering, Morehead State University. In August 2007, he joined Utah State University, Logan, where he is an Assistant Professor of electrical engineering. His research focuses on the applications of micro-nano technologies to a new class of micro-/millimeter-wave circuits and systems, and intelligent wireless communications systems with an emphasis on the multifunctional reconfigurable antennas (MRA) for use in cognitive multi-input multi-output (MIMO) systems. He is the Principal Inventor of three technologies including microwave laminate compatible RF MEMS technology and MRA equipped MIMO systems.

Prof. Cetiner is a member of the IEEE Antennas and Propagation, Microwave Theory and Techniques, and Communication societies.

Gemma Roqueta Crusats (S'08) was born in Girona, Spain, in 1983. She received the Telecommunication Engineer degree from the Technical University of Catalonia (UPC), Barcelona, Spain, in 2007, where she is working toward the Ph.D. degree.

In 2006, she was involved in body area networks research as foreign student in the Catholic University of Louvain, Louvain, Belgium. Since September 2007, she has been with the UPC where she is involved in developing wideband microwave imaging applications for non-destructive quality testing methods for civil structures with fiber reinforcement. Her research interests include indoor and outdoor propagation, wideband microwave imaging, spiralometric discrimination and ultra wide band antennas.

Lluís Jofre (S'79–M'83–SM'07) was born in Mataró, Spain, in 1956. He received the M.Sc. (Ing) and Ph.D. (Doctor Ing.) degrees in electrical engineering (telecommunications eng.), from the Technical University of Catalonia (UPC), Barcelona, Spain, in 1978 and 1982, respectively.

From 1979 to 1980, he was a Research Assistant in the Electrophysics Group,UPC, where he worked on the analysis and near field measurement of antenna and scatterers. From 1981 to 1982, he joined the Ecole Superieure d'Electricite, Paris, France, where he was involved in microwave antenna design and imaging techniques for medical and industrial applications. In 1982, he was appointed Associate Professor at the Communications Department, Telecommunication Engineering School, UPC, where he became Full Professor in 1989. From 1986 to 1987, he was a Visiting Fulbright Scholar at the Georgia Institute of Technology, Atlanta, working on antennas, and electromagnetic imaging and visualization. From 1989 to 1994, he served as Director of the Telecommunication Engineering School (UPC), and from 1994–2000, as UPC Vice-Rector for Academic Planning. From 2000 to 2001, he was a Visiting Professor at the Electrical and Computer Engineering Department, Henry Samueli School of Engineering, University of California. From 2002 to 2004, he served as Director of the Catalan Research Foundation and since 2003 as Director of the UPC-Telefonica Chair. His research interests include antennas, electromagnetic scattering and imaging, and system miniaturization for wireless and sensing industrial and bio applications. He has published more than 100 scientific and technical papers, reports and three books and chapters in specialized volumes.

Necmi Bıyıklı (M'04) was born in Utrecht, The Netherlands, in 1974. He received the B.S., M.S., and Ph.D. degrees in electrical and electronics engineering from Bilkent University, Ankara, Turkey, in 1996, 1998, and 2004, respectively. His M.S. and Ph.D. thesis work concentrated on the design, fabrication and characterization of high-performance photodetectors.

During his Postdoctoral research at the Virginia Commonwealth University, he worked on the growth, fabrication, and characterization of AlGaN/GaN heterostructures for various applications including high-performance GaN/AlGaN transistors. He also worked as a Research Scientist at Utah State University. His research at Utah State University focused on RF-MEMS/NEMS integrated multifunctional reconfigurable antennas. Currently he is with the UNAM – Materials Science and Nanotechnology Institute, Bilkent University. His research interests include RF-MEMS/NEMS integrated reconfigurable antennas, III-Nitride materials and devices for optoelectronic and photovoltaic applications, nanofabrication for novel sensor technologies. He is the author of over 70 citation-index journal papers and refereed conference proceedings.

Dr. Bıyıklı serves as a reviewer for several scientific journals including *Applied Physics Letters*, *IEEE Photonics Technology Letters*, and *IEEE Journal of Quantum Electronics*.